

**Fundamental fouling mechanisms of dissolved organic matter fractions and their implications on the surface modifications of ceramic nanofiltration membranes insights from a laboratory scale application**

Moyo, Welldone; Motsa, Machawe M.; Chaukura, Nhamo; Msagati, Titus A.M.; Mamba, Bhekhe B.; Heijman, Sebastiaan G.J.; Nkambule, Thabo T.I.

**DOI**

[10.2166/wst.2019.419](https://doi.org/10.2166/wst.2019.419)

**Publication date**

2019

**Document Version**

Final published version

**Published in**

Water science and technology : a journal of the International Association on Water Pollution Research

**Citation (APA)**

Moyo, W., Motsa, M. M., Chaukura, N., Msagati, T. A. M., Mamba, B. B., Heijman, S. G. J., & Nkambule, T. I. (2019). Fundamental fouling mechanisms of dissolved organic matter fractions and their implications on the surface modifications of ceramic nanofiltration membranes: insights from a laboratory scale application. *Water science and technology : a journal of the International Association on Water Pollution Research*, 80(9), 1702-1714. <https://doi.org/10.2166/wst.2019.419>

**Important note**

To cite this publication, please use the final published version (if applicable). Please check the document version above.

**Copyright**

Other than for strictly personal use, it is not permitted to download, forward or distribute the text or part of it, without the consent of the author(s) and/or copyright holder(s), unless the work is under an open content license such as Creative Commons.

**Takedown policy**

Please contact us and provide details if you believe this document breaches copyrights. We will remove access to the work immediately and investigate your claim.


***Green Open Access added to TU Delft Institutional Repository***

***'You share, we take care!' – Taverne project***

**<https://www.openaccess.nl/en/you-share-we-take-care>**

Otherwise as indicated in the copyright section: the publisher is the copyright holder of this work and the author uses the Dutch legislation to make this work public.


# Fundamental fouling mechanisms of dissolved organic matter fractions and their implications on the surface modifications of ceramic nanofiltration membranes: insights from a laboratory scale application

Welldone Moyo, Machawe M. Motsa, Nhamo Chaukura, Titus A. M. Msagati, Bhekile B. Mamba , Sebastiaan G. J. Heijman and Thabo T. I. Nkambule

## ABSTRACT

This work reports on the fundamental factors influencing inter-foulant and foulant-membrane interactions during simulated dissolved organic matter removal using ceramic nanofiltration. Fouling tests were performed using sodium alginate (SAL), humic acid (HA) and bovine serum albumin (BSA) as model foulants. Fouling potentials of each foulant and their mixtures were investigated using feed solutions containing fixed concentrations of  $K^+$ ,  $Na^+$ ,  $Mg^{2+}$  and  $Ca^{2+}$  with a total ionic strength of 10 mM. The impact of modification by atomic layer deposition on fouling mitigation was also assessed. The flux decline in the first 100 min for single foulants was  $4.16 \times 10^{-2}$ ,  $2.69 \times 10^{-2}$  and  $1.60 \times 10^{-2} \text{ Lm}^{-2}$  for SAL, HA and BSA, respectively. These results demonstrated that for the single foulants, deposition on the membrane surface in the early stages of filtration was primarily governed by membrane-foulant interactions. Interestingly, cake filtration was the least fouling mechanism in feed solutions composed of BSA and SAL ( $R^2 = 0.519$ ,  $0.374$  for BSA + SAL and BSA + SAL + HA, respectively) and the most favorable fouling mechanism of feed solution which included HA and SAL ( $R^2 = 0.972$ ). The water contact angle dropped from  $58^\circ$  to  $35^\circ$  after coating, thus improving its anti-fouling properties.

**Key words** | atomic layer deposition, ceramic membrane, dissolved organic matter, membrane fouling, nanofiltration

Welldone Moyo  
Machawe M. Motsa  
Nhamo Chaukura  
Titus A. M. Msagati  
Bhekile B. Mamba   
Thabo T. I. Nkambule (corresponding author)  
Nanotechnology and Water Sustainability  
(NanoWS) Research Unit,  
University of South Africa (UNISA),  
Johannesburg,  
South Africa  
E-mail: [nkambtt@unisa.ac.za](mailto:nkambtt@unisa.ac.za)

Sebastiaan G. J. Heijman  
Department of Civil Engineering and GeoSciences,  
Technical University of Delft,  
Delft,  
The Netherlands

## INTRODUCTION

There is a continual deposition and accumulation of organic and inorganic substances in the aquatic systems as a result of both natural and anthropogenic activities. With water scarcity and an increase in industrial activities, the concentration of these compounds and other emerging micropollutants is intensified, thus compromising the quality of the natural water streams. Dissolved organic matter (DOM) is one class of pollutants found in abundance in water sources (Nkambule 2012). Previous studies have reported that DOM compromises the quality of water by giving it color, bad odor and a foul taste (Chaukura *et al.* 2018). Because of this, there is a need to monitor and remove DOM and its fractions in drinking water. One treatment approach that has

shown good success in removing DOM in water is membrane technology. However, one of the enduring challenges of membrane processes is fouling.

While studies on membrane fouling mechanisms are well documented in the case of polymeric membranes (e.g. Mahlangu *et al.* 2015a, 2015b; Shang *et al.* 2015; Shen & Schaffer 2015), conflicting reports on DOM fractions contributing more to membrane fouling have been reported. Some studies report that colloidal DOM fraction contributes more to membrane fouling than other fractions (Kim & Dempsey 2013). Other studies reported that aromatic or hydrophobic compounds (humic and fulvic acids) were the major DOM foulants on ultra and nanofiltration membranes

(Rubia et al. 2008). Besides, polysaccharides have been reported to contribute more to membrane fouling (Mahlangu et al. 2015a, 2015b). Furthermore, macromolecular biopolymers such as dextran and sodium alginate increase the severity of fouling, especially in the presence of inorganic particles (Yamamura et al. 2014). Interestingly, the presence of inorganic particles alone has no effect on the severity of membrane fouling (Yu et al. 2015). Many simulation studies have focused on investigating the fouling behavior of polymeric membranes by mono-dispersed foulants, which have homogeneous physico-chemical properties and a defined character (Motsa et al. 2015). However, investigations of fouling by mono-dispersed foulants cannot be reliably extrapolated to field applications where foulants exist as mixtures, and fouling cannot be attributed to a single foulant.

Although ceramic materials have been introduced in the water treatment industry more than a decade ago, little is known about their fouling behavior by organic macromolecules. Therefore, in order to advance the use of ceramic membranes in water treatment, it is important to understand the fundamental fouling mechanisms involved during the filtration process. The commonly used fabrication method for ceramic membranes is the sol-gel method. However, this method returns a challenge in the development of tight ceramic nanofiltration (NF) membranes. Atomic layer deposition (ALD), a gas-solid phase coating procedure for growing atomic-scale thin films, is a potential route to address sol-gel fabrication deficiencies and for modifying ceramic membranes (Shang et al. 2017). The surface reactions of ALD result in exquisitely uniform and conformal pinhole-free 3-D coatings of metal oxides on the membrane surface and pore walls, resulting in predetermined pore size. For instance, TiO<sub>2</sub> loose NF membranes fabricated by the sol-gel method were tuned from a pore size of 20 to 1 nm via the ALD method (Song et al. 2016). Intriguingly, the clean water permeability of the ALD-modified NF membranes almost doubled that of the unmodified sol-gel-made NF membranes (Puhlfürß et al. 2000). The ALD modified membranes show promise in increased water permeability; however, there is no reported study to demonstrate the impact or mechanism of fouling on these membranes compared to the pristine (unmodified) membranes. Consequently, this research study focuses on identifying the contributions of each DOM fraction in permeate flux decline during ceramic membrane filtration. The purpose of this research was to investigate, model, and identify the contributions of each DOM fraction (humic acid, bovine serum albumin, and sodium alginate) in permeate flux

decline at pilot scale during ceramic membrane filtration of ALD-modified membranes and compare them with the pristine membranes. The reduction in permeate flux was modelled using the FEEM-PARAFAC model.

## MATERIALS AND METHODS

### Materials

Analytical grade reagents were used and were purchased from Sigma Aldrich, South Africa. Deionized (DI) water (Milli-Q, Millipore, USA) was used for all experiments. Humic acid (HA) (50 mg/L), bovine serum albumin (BSA) (20 mg/L), and sodium alginate (SAL) (30 mg/L) were used as model dissolved components of organic matter; humus substances, protein-like and polysaccharide-like substances, respectively (Table 1) (Angelis et al. 2013; Mahlangu et al. 2015a, 2015b; Schulz et al. 2016). To make up the ionic strength of the solutions to 10 mM, NaCl, KCl, CaCl<sub>2</sub>, and MgCl<sub>2</sub> were used as background electrolytes. While these concentrations are above those in surface waters (Sun et al. 2016), they mimic foulant concentrations after extended operation. All experiments were carried out at room temperature, and membranes were used as received from the manufacturer without any further pretreatment.

### Membranes characterization

#### Substrate membranes

Commercial ceramic NF membranes purchased from TAMI, France, were used in these experiments. The membranes had a disc configuration of 90 mm diameter, 2.5 mm

**Table 1** | Compositions of the various feed solutions tested during filtration experiments ( $n = 3$ )

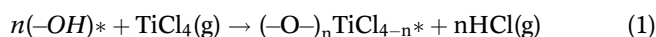
Feed solution	DOC concentration (mgL <sup>-1</sup> )	pH	Turbidity (NTU)	Conductivity (μSm <sup>-1</sup> )
SAL	13	6.08	0.65	935
BSA	7	5.08	0.68	688
HA	18	6.69	18.88	442
SAL + BSA	27	5.9	0.00	973
SAL + HA	18	6.1	17.89	1,237
BSA + HA	22	5.8	16.21	449
SAL + BSA + HA	35	8.5	14.01	1,132

BSA – bovine serum albumin; HA – humic acid; SAL – sodium alginate; DOC – dissolved organic matter.

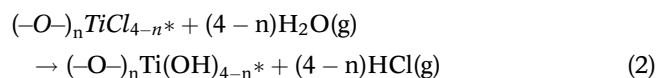
thickness, and an effective filtration area of 0.00563 m<sup>2</sup>, with a porosity of 30% and MWCO of 450 Da. The active and support layer of the as-received membrane was made of TiO<sub>2</sub> and Al<sub>2</sub>O<sub>3</sub>, respectively. A field emission scanning electron microscope (JSM-IT300, JEOL, Oxford, UK) with an energy dispersive X-ray detector was used to analyse the surface morphology and elemental mappings of the membrane.

### Modification of ceramic membranes via the atomic layer deposition

Coating TiO<sub>2</sub> onto substrates was achieved by the use of a flow-type ALD reactor (TU Delft, The Netherlands). The precursors for this reaction were TiCl<sub>4</sub> (Sigma-Aldrich/Fluka, The Netherlands) and demineralized water vapor. Nitrogen gas (HiQ 5.0, Linde Gas Benelux, The Netherlands) was used as a carrier for the diluted precursors. An infrared lamp connected to a digital temperature probe was used to heat up the ALD reactor to an operating temperature of 70 °C. The gaseous precursors deposited on the substrate in a direction perpendicular to its surface. Upon exposure to the substrate, TiCl<sub>4</sub> chemisorbed following Equation (1) (Shang et al. 2017):



The asterisk denotes the surface species. Thereafter, dry N<sub>2</sub> was used to purge the excessive TiCl<sub>4</sub> and produced HCl vapors. Then the co-reactant water vapour was introduced into the chamber to complete one cycle of coating (Equation (2)) (Shang et al. 2017):



Residual H<sub>2</sub>O and produced HCl vapors were then purged off using dry N<sub>2</sub>. The process was carried out to obtain two coats to keep the pore sizes close to the unmodified membranes so that the only variable for comparison was surface modifications.

### Contact angle

Contact angles were measured using the sessile drop method whereby three liquids (Milli-Q water, diiodomethane and glycerol) with well-characterized surface tension components were used. A microlite syringe was used to place at least 10 drops per liquid on the membrane. The contact

angle was then determined (mean ± standard deviation). Surface tension and interfacial free energies of interactions was then calculated from the contact angles value.

### Membrane surface energetics

In this study, water, glycerol, and diiodomethane were used as probe liquids. In-depth characterization and measurements of these liquids are reported elsewhere (Motsa et al. 2014). In brevity, the total surface tension component of any material is the sum of the Lifshitz-van der Waals component ( $\gamma^{LW}$ ) and Lewis acid–base components  $\gamma^{AB}$  ( $\gamma^{AB} = 2\sqrt{\gamma^+\gamma^-}$ ) with  $\gamma^+$  and  $\gamma^-$  being the electron acceptor and electron donor, respectively (Equation (3)):

$$\gamma^{TOT} = \gamma^{LW} + \gamma^{AB} \quad (3)$$

Using the three liquids of known surface tension to measure the contact angles ( $\theta$ ) makes the calculation of  $\gamma^{LW}$ ,  $\gamma^+$  and  $\gamma^-$  possible using Young-Dupree equation (Equation (4)) (Motsa et al. 2015):

$$\left(1 + \frac{\cos\theta}{r}\right)\gamma_s^{TOT} = 2\left(\sqrt{\gamma_s^{LW}\gamma_i^{LW}} + \sqrt{\gamma_s^+\gamma_i^-} + \sqrt{\gamma_s^-\gamma_i^+}\right) \quad (4)$$

where  $r$  accounts for the increase in surface area due to membrane roughness, subscripts  $i$  and  $s$  are the test liquid and solid surface, respectively.

### Concentrate and permeate characterization

#### Fluorescence and DOC measurements

Parafac modeling using the SOLO software (Eigenvector Inc., USA), which is inbuilt in the fluorescence spectrometer, Aqualog (HORIBA Jobin Yvon), was used to quantify the foulants in the feed water and in the permeate. The quantitative distribution of the components after each treatment stage was determined using their maximum fluorescence intensities ( $F_{max}$ ). An in-depth treatment of the Parafac model can be accessed in Ndiweni et al. (2019). Triplicate DOC measurements for all samples were determined using a total organic carbon analyzer (TOC fusion, Teledyne Tekmar). The TOC analyzer was calibrated using potassium hydrogen phthalate (KHP), and instrument performance was assessed by placing additional KHP standards along with, and in the same manner as, the samples. These ‘check standards’ were within 2.5% of their known concentrations.

## Filtration operation and fouling model mechanisms

The different feed solutions (Table 1) were circulated by a pump operated at 1,100–1,180 RPM. The membrane was housed in a circular disc membrane module (TAMI, Germany), and the system was pressurized by altering the concentrate valve. Measurements were run under an operational pressure of 3 bar and a feed flow of 175 L/h in cross flow mode. During pure water permeability tests, measurements were done at 10 min intervals to determine initial permeate flux and until the flux stabilized. During fouling tests, the permeates were collected after every 5 min for the first 2 h, then after every 10 min for the subsequent 2 h, thereafter after every 30 min for another 2 h, then ultimately per hour for the last 2 h. The impact of each foulant on permeate flux and the fouling behavior was investigated by filtering the foulants in the presence of  $\text{Na}^+$ ,  $\text{K}^+$ ,  $\text{Mg}^{2+}$  and  $\text{Ca}^{2+}$ .

The flow rate was correlated to the sample mass, and the flux and temperature-corrected permeability were determined (Box 1) (Shang et al. 2017):

### Box 1 | Mass flow equations

$$v_s = \frac{(M_{sc} - M_c)}{(T_f * 60)/1000}$$

$$\Delta P = \frac{P_f + P_c}{2}$$

$$J = \frac{v_s}{A}$$

$$L_{p,20^\circ\text{C}} = \frac{J}{\Delta P} \cdot \frac{\eta_T}{\eta_{20}} = \frac{J \cdot e^{-0.0259 \cdot (T-20)}}{\Delta P}$$

Where  $v_s$  is the flow rate,  $M_{sc}$  and  $M_c$  is the mass (g) of the sample container plus permeate sample and the mass (g) of the empty container respectively,  $T_f$  is the temperature of water ( $^\circ\text{C}$ ),  $\Delta P$  is the measured TMP (bar),  $P_f$  (bar) is the feed pressure and  $P_c$  (bar) is the concentrate pressure,  $J$  is the measured membrane flux ( $\text{Lm}^{-2}\text{h}^{-1}$ )  $A$  is the effective membrane filtration area,  $L_{p,20^\circ\text{C}}$  is the permeability at  $20^\circ\text{C}$  ( $\text{Lm}^{-2}\text{h}^{-1}\text{bar}^{-1}$ ) and  $\eta_{20}$  and  $\eta_T$  are the permeate viscosity at  $20^\circ\text{C}$  and at the measured water temperature.

The fouling mechanisms were determined using the model equations in Box 2:

### Box 2 | Models to describe fouling mechanisms: (1) complete blocking, (2) standard blocking, (3) intermediate blocking, and (4) cake filtration, respectively (Angelis et al. 2013)

$$(1) J = J_0 e^{-At} \quad A = K_A u_0$$

$$(2) J = \frac{J_0}{(1 + Bt)^2} \quad B = K_B u_0$$

$$(3) J = \frac{J_0}{(1 + At)}$$

$$(4) J = \frac{J_0}{\sqrt{1 + Ct}} \quad C = (2R_r)K_C u_0$$

Where  $J_0$  and  $J$  are initial and final flux respectively;  $u_0$  average initial filtrate velocity;  $R_r$  is the ratio of resistance of the cake to the clean membrane;  $K_A$  is membrane surface blocked per unit of total volume permeated through the membrane;  $K_B$  is decrease in cross-section area of the pores due to the particles deposited on the walls per unit of total permeate volume;  $K_C$  is total permeate volume per unit of membrane area.

After operation membranes were chemically cleaned by soaking for 7 h in 0.1%  $\text{NaClO}$ , thereafter rinsed in DI water and then clean water permeability followed.

## RESULTS AND DISCUSSION

### Fouling characteristics of single foulants on the pristine membranes

#### Permeate flux loss due to single foulants on the pristine membranes

Permeate flux drop caused by alginate was drastic (54%) (Figure 1), indicating severe membrane fouling, and is in good agreement with similar reports of other SAL fouling studies (Motsa et al. 2018). Compelaxation with cations could have enhanced the SAL–SAL interactions, leading to their subsequent deposition on the membrane surface. In the early filtration stage, flux decline decreases drastically at a rate of  $4.16 \times 10^{-2} \text{Lm}^{-2}$  in the first 100 min. Thus, the interplay of permeation drag force generated in the early stages of the filtration process and membrane–SAL interactions promoted the adhesion of SAL onto the membrane surface (Mahlangu et al. 2015a, 2015b).

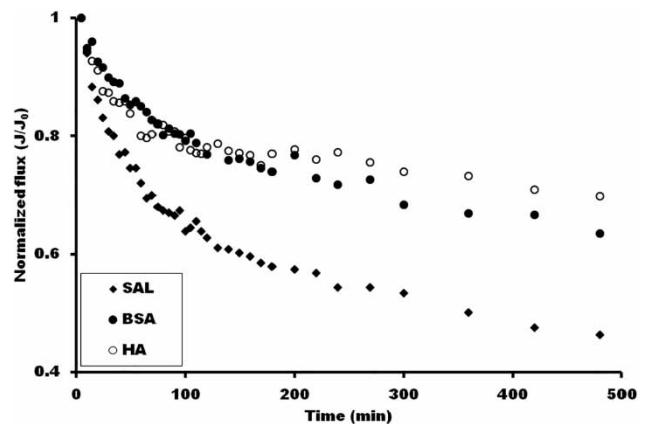


Figure 1 | Permeate flux loss due to single model organic foulants on the pristine membrane. BSA – bovine serum albumin; HA – humic acid; SAL – sodium alginate.

The presence of cations promotes the formation of alginate-cation aggregates, which in turn were responsible for the flux decline and its severity was increased with the increases in the effective size of the alginate molecules. HA-calcium complexes have been shown to form in the presence of  $\text{Ca}^{2+}$ , and can intensify the HA fouling (Metsämuuronen et al. 2014). Moreover, it has been shown that HA is not especially selective to  $\text{Ca}^{2+}$  cations alone. In this case, other cations ( $\text{Na}^+$ ,  $\text{K}^+$  and  $\text{Mg}^{2+}$ ) were present, which competed for the negative charges in HA, resulting in the formation of varying sizes of HA aggregates that were not easily deposited onto the membrane surface (Metsämuuronen et al. 2014). In the early filtration stage, flux decline decreased moderately at a rate of  $2.69 \times 10^{-2} \text{ Lm}^{-2}$  in the first 100 min (Figure 1). Permeation drag force generated in the early stages of the filtration process and membrane-HA interactions could have promoted the adhesion of HA onto the membrane surface at differential rates. The deposition of HA onto the membrane was moderately stable after the initial 100 min of flux decline, suggesting the small HA-cation aggregates did not favorably form a multilayered structure which would result in increased flux decline.

Membrane fouling due to BSA deposition showed a flux decline rate of  $1.60 \times 10^{-2} \text{ Lm}^{-2}$  in the first 100 min. Permeate flux remained stable due to the inability of the deposited monolayer of the less negative BSA having a negligible effect on the membrane flux. However, as the filtration progressed permeation drag formed a multi-layered film of protein on the membrane that provided resistance to the permeate flow. It can therefore be conjectured that a multi-layered film was built up by the interactions between adsorbed BSA molecules and incoming molecules, and BSA-membrane interactions were at play at the initial stages of the macromolecular adsorption. Polysaccharides and protein-like fractions have been reported to be responsible for severe membrane fouling during wastewater treatment, thus corroborating our findings (Zularisam et al. 2007). The results demonstrated that, for the single foulants, foulant deposition on the membrane surface in the early stages of filtration was primarily governed by membrane-foulant interactions.

### Modeling fouling mechanisms of single foulants on the pristine membranes

The SAL filtration experiments showed a sharp drop in flux from the beginning, to almost 33% of the initial flux after only 100 min of filtration. Similar behavior was reported for SAL filtration with polymeric membranes, and was associated with the rapid formation of a gel-like layer that presents an extra

resistance to water permeability (Kim & Dempsey 2013). Interpretation of the experimental data with the mechanistic models for SAL (Figure 2(1a)–2(1d)) are consistent with the cake filtration mechanism ( $R^2 = 0.985$ ) preceded by intermediate blocking ( $R^2 = 0.964$ ), where pores on the surface are blocked by particles but also deposit onto each other. The initial large decay observed in the flux evolution with time ends at this point, and a considerably slower reduction of permeability begins. The mechanistic fouling models showed cake filtration as the predominant fouling mechanism, thus supporting our findings. Due to the bigger size of the aggregates formed during SAL- $\text{Ca}^{2+}$  complexation, a loose, rather permeable gel layer is formed on the surface.

In BSA filtration, experimental data adjusted well to standard ( $R^2 = 0.937$ ) intermediate blocking ( $R^2 = 0.956$ ) and ultimately complete blocking ( $R^2 = 0.941$ ) mechanisms, indicating adsorption onto the inner pores of the membrane. It is interesting to note that cake filtration was the least likely mechanism of fouling ( $R^2 = 0.899$ ) (Figure 2(2a)–2(2d)).

HA fouling mechanisms had almost equal occurrence for complete blocking, standard blocking, and intermediate blocking ( $R^2 = 0.873$ ; 0.869 and 0.833 respectively) (Figure 2(3a)–2(3d)). These results suggest equal interplay of these fouling mechanisms. However, it could not be established whether these fouling mechanisms occurred sequentially or concurrently. The deposition of small HA-cation aggregates formed a somehow soft cake layer without further forming multilayers and did not alter the rate of flux decline.

### Permeate flux loss due to single foulants tracked by FEEM-PARAFAC model on the pristine membranes

Because HA and BSA fluoresce in the UV-Vis regions (Shao et al. 2014), it was possible to follow their filtration progress using fluorescence excitation emission matrix spectroscopy. The quantification of the foulants in the concentrate and permeate was followed using the inbuilt SOLO software for PARAFAC analysis (Figure 3). As expected, the fouling behavior of BSA was constant in the first 120 min as depicted by minimum fluctuations of the  $F_{max}$  of the concentrate. There was a decrease in the  $F_{max}$  signal of the permeate, suggesting less BSA was permeating through the membrane barrier after 180 min through to 300 min of filtration. This implies more protein molecules were deposited on the adsorbed BSA monolayer due to BSA-BSA interactions, forming a multi-layered film that provided resistance to permeate flow (Figure 3(a)). There was a shift in  $F_{max}$  after 300 min through to the end of the filtration run, suggesting a change in the fouling mechanism. This staged filtration

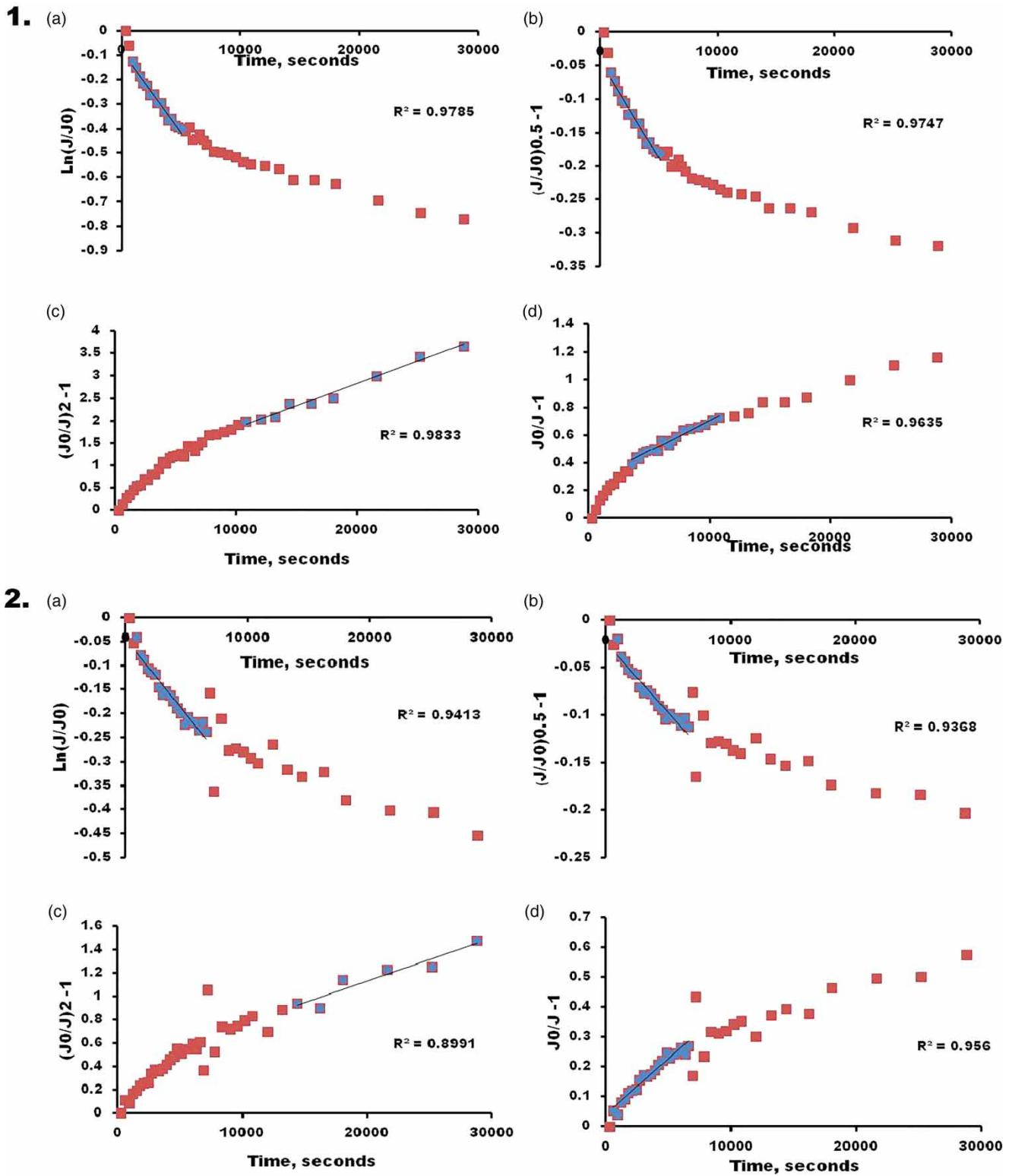


**Figure 2** | Mechanistic fouling of single foulants on the pristine membrane – 1: SAL; 2: BSA; 3: HA and modified membrane; 4: SAL. Where (a) is complete blocking, (b) is standard blocking, (c) is cake filtration, (d) is intermediate fouling. BSA – bovine serum albumin; HA – humic acid; SAL – sodium alginate. (Continued.)



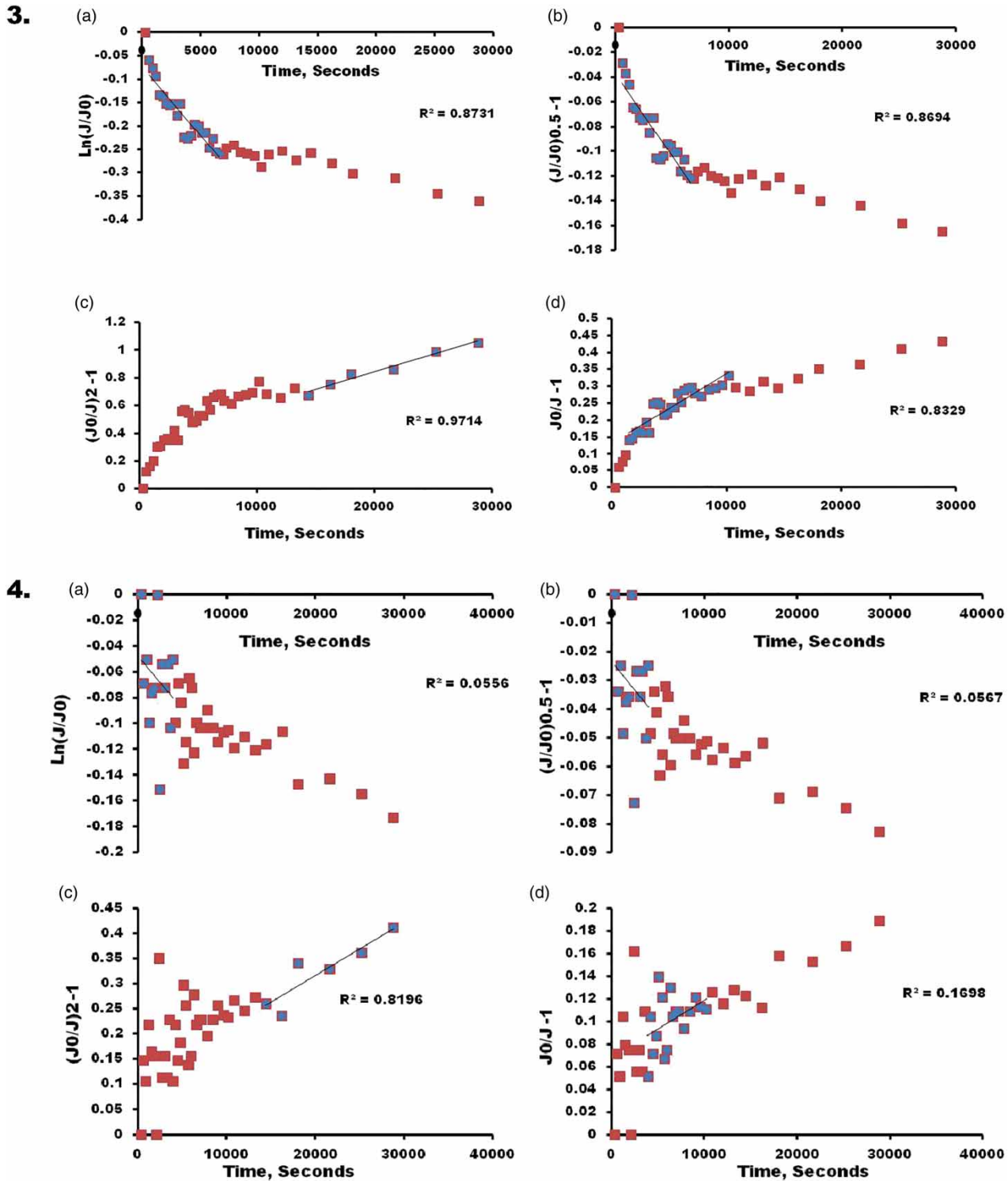
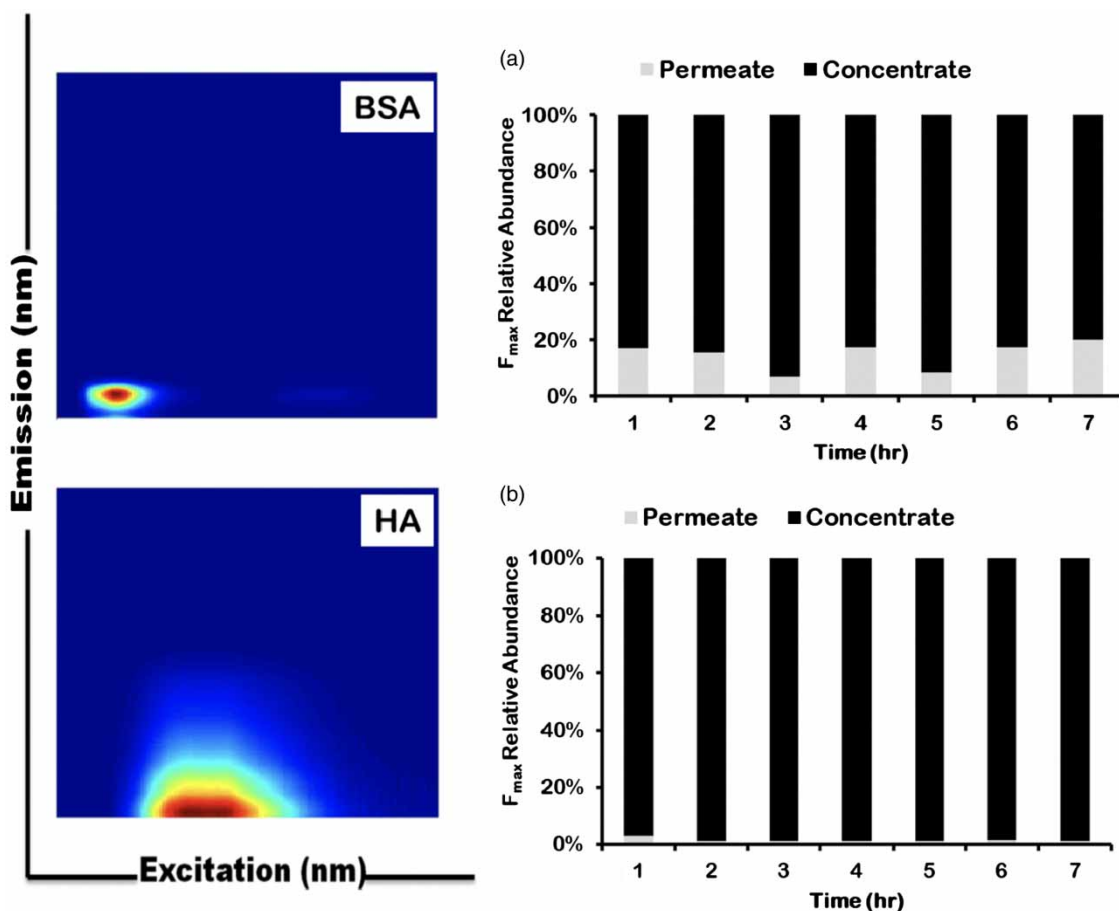


Figure 2 | Continued.

character of BSA has been reported by *Motsa et al. (2018)*. Little variation of  $F_{max}$  was observed for HA throughout the filtration run, although the  $F_{max}$  signal is greater in the

concentrate and almost consistent throughout the filtration run (*Figure 3(b)*). This result is consistent with previous reports and our findings that the presence of  $\text{Ca}^{2+}$  ions



**Figure 3** | EEM contours of model foulants identified by PARAFAC and their relative abundance in the concentrate and in the permeate of the pristine membrane. (a) BSA component and (b) HA component. BSA – bovine serum albumin; HA – humic acid.

chelates with HA forming aggregates that do not easily settle nor easily pass through the membrane barrier (Angelis *et al.* 2015; Shao *et al.* 2014; Wang *et al.* 2017).

The fraction of NOM that fluoresces in the UV-Vis range is referred to as fluorescent natural organic matter (fNOM). Because they are the main components of membrane fouling, the fNOM fractions important to NF are proteins and humic substances (Shao *et al.* 2014). Therefore, fluorescent NOM fractions have to be monitored and controlled in NF membrane operations.

### Effect of foulant mixtures on the pristine membranes

#### Permeate flux loss due to combined foulants on the pristine membranes

The combinations of HA + SAL + BSA and HA + SAL followed a similar trend with 22 and 25% flux loss, respectively within the first 100 min (Figure 4). SAL and

BSA caused 38 and 20% flux loss, respectively, in the same duration. The presence of SAL with other foulants reduced its fouling propensity, probably because of the competitive effect of the foulants for cations. The cations concentration was far less compared to the foulants concentrations, therefore SAL complexation was minimal, and the bulk of SAL remained in solution instead of aggregates that could settle on the membrane surface, resulting in lower flux loss compared to SAL alone. A summary of the experimental  $R^2$  values is shown in Table 2. It was interesting to note that cake filtration was the least fouling mechanism in feed solutions containing BSA and SAL ( $R^2 = 0.519, 0.374$  for BSA + SAL and BSA + SAL + HA, respectively), this finding is contrary to reported literature, whereby such mixtures supported cake filtration since the BSA macromolecules are incorporated into the SAL-cation complexes (Nguyen *et al.* 2012). The most favorable fouling mechanism of cake filtration was of a feed stream containing HA and SAL ( $R^2 = 0.972$ ); this can be explained by the complexation

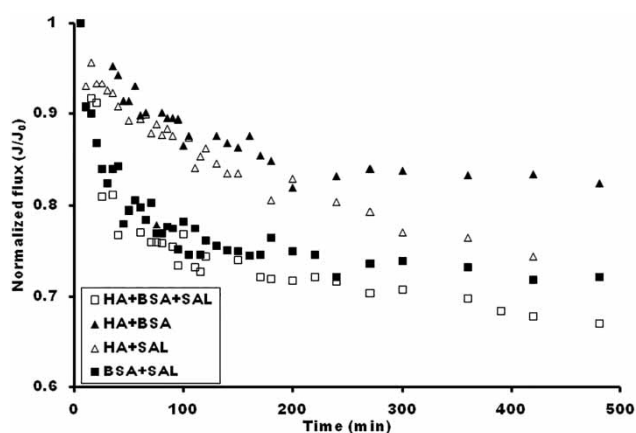


**Figure 4** | Permeate flux loss profiles due to combined foulants on the pristine membrane. BSA – bovine serum albumin; HA – humic acid; SAL – sodium alginate.

of cations to the organics due to the formation of large HA-cation, SAL-cation and SAL-HA complexes which settle on the surface of the membrane and increase the resistance to permeate flow. Permeate flux loss was enhanced by the deposition of these large aggregates via permeation drag forming a layer that also reduced the back-diffusion of salts from the membrane surface to the bulk solution. However, previous studies showed that the surface charges of these foulants are negative, and should repel each other (Nguyen *et al.* 2012). Depending on the magnitude of the negative charge, the formation of combined macromolecular structures is hindered due to charge repulsion. The presence of cations then necessitates the formation of smaller aggregates on a competitive basis that do not easily settle on the surface of the membrane, thus keeping the cake filtration effect to a minimum.

The combination of BSA + HA and BSA + SAL resulted in a flux loss of 15 and 25%, respectively, whereas the flux loss of individual HA and SAL was 21 and 54%, respectively. Again, of interest in this study was that dual combinations containing BSA favored the complete

blocking fouling mechanism ( $R^2 = 0.848$ ; 0.78 for BSA + HA and BSA + SAL respectively), and standard blocking fouling mechanism ( $R^2 = 0.85$ , 0.75 for BSA + HA and BSA + SAL respectively) (Figure S1, Supplementary Information). These results suggest the presence of BSA disrupts the formation of large macromolecular structures of organic-cation and organic-organic complexes. This could be because BSA has a larger charge density and smaller size, attracting more positive charge to itself and leaving the bulkier HA and SAL in solution. The trend in flux loss was strikingly similar to that of BSA alone, exhibiting a two-stage fouling behavior. Firstly, there was a rapid flux loss from the onset to about 200 min for BSA + HA, and 150 min for BSA + SAL, followed by a steady state flux through to the end of the experiment.

Even though the single and dual combination of HA and SAL favored cake filtration ( $R^2 = 0.971$ ; 0.985; 0.972 for HA; SAL and HA + SAL, respectively) (Table 2, Figure S1), and the flux loss of 21; 54 and 25% for HA; SAL and HA + SAL, respectively, the co-existence of HA and SAL in the feed reduced the fouling propensity of SAL on its own. This could be attributed to competition for cations in solution, with HA attracting more positively charged species than SAL, thus leaving most of SAL in solution. The resulting trend in flux loss for the combined HA + SAL is dissimilar to the constituent foulants. The trend for HA + SAL fouling showed an almost linear decline, whereas single foulants showed a two-part fouling behavior. Initially, a rapid flux decline was exhibited, followed by an almost steady state flux towards the end.

### Influence of membrane surface modification on flux decline

The impact of membrane surface modification was studied with feed solutions that caused the most severe fouling on the pristine membranes, namely: SA and HA + BSA + SAL

**Table 2** | Summary of the  $R^2$  of the mechanism of fouling for single and combined foulants

	Unmodified membrane							Modified membrane	
	SAL	HA	BSA	HA + SAL	HA + BSA	BSA + SAL	SAL + HA + BSA	SAL	SAL + HA + BSA
Complete blocking	0.979	0.873	0.941	0.804	0.848	0.780	0.761	0.056	0.744
Standard blocking	0.975	0.869	0.937	0.801	0.850	0.750	0.750	0.057	0.739
Cake filtration	0.983	0.971	0.899	0.972	0.454	0.519	0.374	0.820	0.992
Intermediate blocking	0.964	0.833	0.956	0.800	0.699	0.572	0.598	0.170	0.392

BSA – bovine serum albumin; HA – humic acid; SAL – sodium alginate.

(Figure 5). The rate of flux decline (25%) was similar for both membranes in the first 50 min with SA as the foulant, thereafter a steady state flux was observed for the coated membrane. However, a declining flux trend was exhibited by the pristine membrane (Figure 5(a)). The modification of the membranes improved flux loss by 35% when SAL was the foulant. For both types of membranes, cake filtration was the favored fouling mechanism ( $R^2 = 0.985$  and  $0.8196$  for the pristine and coated membranes, respectively). These results suggest modification improved the anti-fouling property of ceramic membranes. Inherent to the ceramic membrane surface is the presence of the negatively charged OH group (Kim & Jang 2016). It appears coating introduced more OH groups onto the surface of the membrane, resulting in greater electrostatic repulsion of SAL.

However, there was no significant difference when foulants were combined in the feed. In fact, the pristine membrane performed better than the coated membrane by a 5% difference of the resultant flux decline (Figure 5(b)). The fouling mechanism was almost similar for both membranes. For the coated membrane,  $R^2 = 0.744$ ;  $0.7388$  and  $0.3962$  for complete blocking, standard blocking, and intermediate blocking, respectively, while for the pristine membrane,  $R^2 = 0.761$ ;  $0.75$  and  $0.598$  for complete blocking, standard blocking, and intermediate blocking, respectively. Cake filtration was the favored fouling mechanism for the coated membrane ( $R^2 = 0.9916$ ), whereas cake filtration was the least favored fouling mechanism for the pristine membrane ( $R^2 = 0.374$ ). The cations have been reported to act as bridges between the increased OH groups introduced by coating and the foulants in the feed solution, thus promoting the sedimentation of foulants onto the coated membrane (Kim & Jang 2016).

## Fundamental differences brought about by modification

### Contact angle

Upon additional deposition of  $\text{TiO}_2$  layers on the membrane surface, the measured water contact angles dropped from  $58^\circ$  to  $38^\circ$  (Figure S2, Supplementary Information), indicating the improved water affinity. This means the membrane could be easily wetted by water during filtration, which has a positive impact on mass transfer (water transport) and weakens the adhesion forces between the membrane surface and foulants. The anti-fouling properties are thus improved. This observation was further complemented by the surface free energies for the two membranes (Table 3). After atomic layer deposition of  $\text{TiO}_2$ , the membrane hydrophilicity was enhanced by the addition of more OH groups. In general terms, surface hydrophilicity/hydrophobicity has been defined by the value of the measured contact angle; with an angle of less than  $90^\circ$  considered hydrophilic, with  $90^\circ$  and above regarded as hydrophobic.

### Surface energetics

All the membranes had a strong electron donor monopolarity (Table 3). The values of the surface free energy components correlated with the measured water contact angles. The pristine membranes had a slightly higher Lifshitz-van der Waals component, which corresponds to the contact angle of the apolar liquid, diiodomethane, thus the inclined water contact angle. The computed value of the acid-base ( $\gamma^{\text{AB}}$ ) component, which is an indicator for hydrophilicity was  $6.62$ , which increased to  $9.06$  upon coating with  $\text{TiO}_2$ , confirming the increase in surface hydrophilicity. The deposition of  $\text{TiO}_2$  creates favorable interactions between the

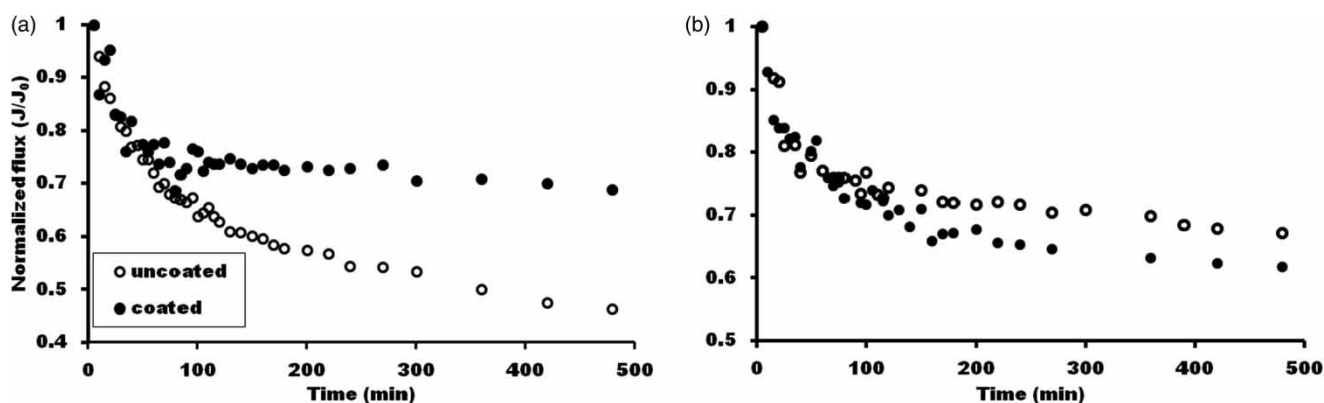


**Figure 5** | Comparison of fouling profiles of coated and pristine membranes due to (a) SAL foulant and (b) HA + BSA + SAL. BSA – bovine serum albumin; HA – humic acid; SAL – sodium alginate.

**Table 3** | Surface free energy components for the unmodified and modified membrane samples

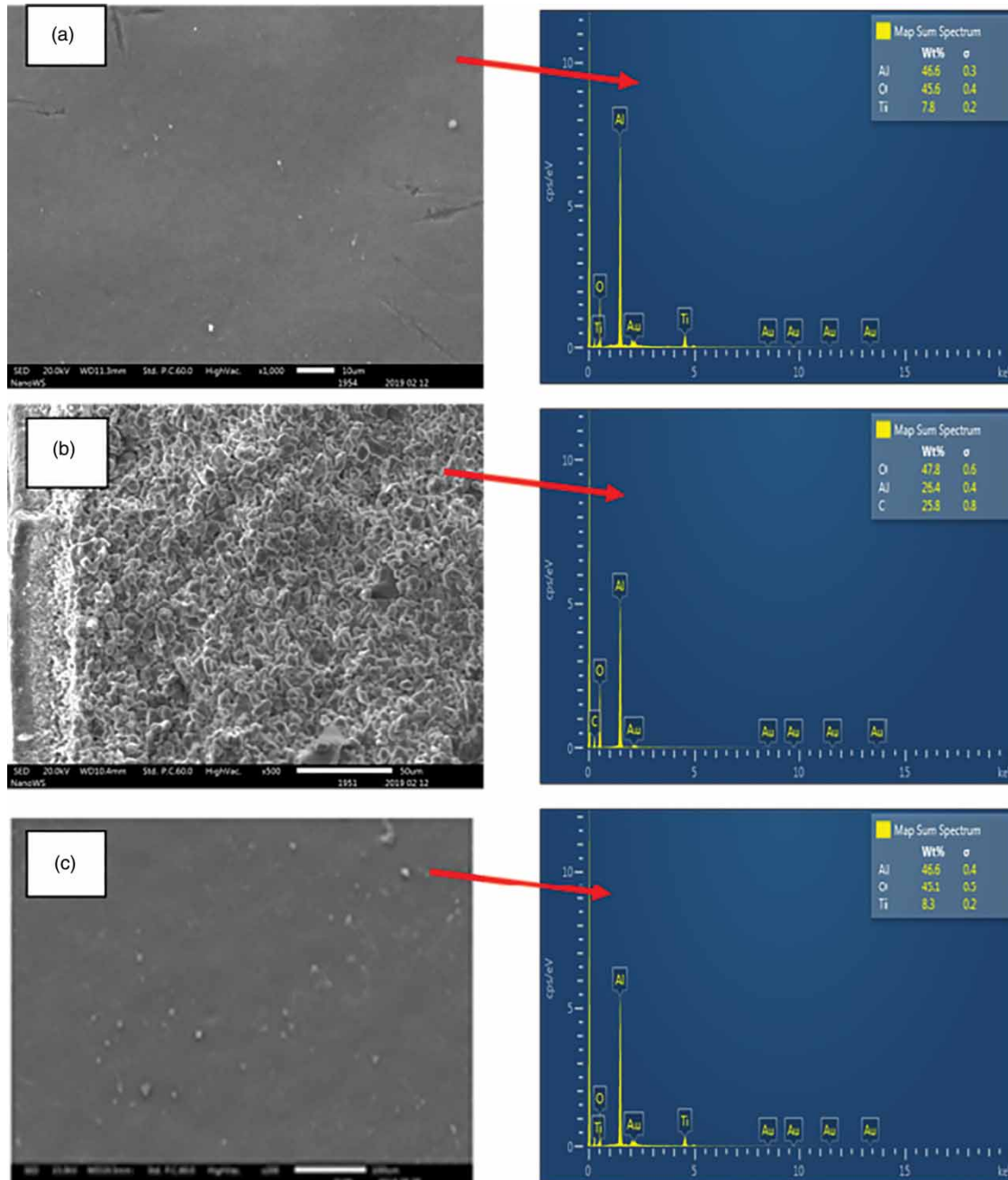
	Surface free energy components				
	$\gamma^{LW}$	$\gamma^+$	$\gamma^-$	$\gamma^{AB}$	$\gamma^{TOT}$
Pristine	38.57	0.24	45.09	6.62	45.20
Coated	35.30	0.36	56.69	9.06	44.36

$\gamma^{LW}$  – Lifshitz-van der Waals component;  $\gamma^{AB}$  Lewis acid–base component;  $\gamma^+$  – electron acceptor and  $\gamma^-$  – electron donor; and  $\gamma^{TOT}$  – ( $\gamma^{LW} + \gamma^{AB}$ )

membrane surface and water molecules, which subsequently lowers the adhesion forces between on-coming foulants and the membrane surface, thus limiting fouling propensity.

### Surface elemental composition

The scanning electron microscopy (SEM) imaging and energy dispersive X-ray spectroscopy (EDS) mapping

**Figure 6** | Surface elemental composition of the (a) top side of the coated membrane, (b) cross section of the coated membrane and (c) top side of the pristine membrane.

(Figure 6) of the coated and pristine membranes indicates that the membrane consists of a porous support that contains a significant amount of Al. The selective layer showed the presence of both Al and Ti, confirming that the ALD process deposited an ultrathin layer on the surface. Interestingly, the cross-sectional elemental analysis of the coated membrane did not show any presence of Ti as a constituting element, thus confirming pore constriction did not occur (Figure 6(b)). Hence, the observed change in water affinity was mainly due to favorable interactions between the TiO<sub>2</sub> on the active layer and water molecules, which subsequently led to enhanced anti-fouling properties.

## CONCLUSION

The contributions of each DOM fraction and their combinations (SAL, HA and BSA) in permeate flux decline during ceramic membrane filtration was investigated in this study. The effect of membrane surface modification on fouling resistance was studied by comparing the performance of both TiO<sub>2</sub> ALD coated and pristine membranes. The results showed that SAL caused the most extensive fouling on pristine membranes and coating reduced its fouling potential by 35%. Cake filtration was the least fouling mechanism in feed solutions composed of BSA and SAL, and the most favorable fouling mechanism of feed solution which included HA and SAL. The fouling mechanisms were almost similar for both membranes. For the coated membrane,  $R^2 = 0.744$ ; 0.7388 and 0.3962 for complete blocking, standard blocking and intermediate blocking, respectively whilst for the pristine,  $R^2 = 0.761$ ; 0.75 and 0.598 for complete blocking, standard blocking, and intermediate blocking, respectively. However, cake filtration was the favored fouling mechanism for the coated membrane ( $R^2 = 0.9916$ ), and the least favored fouling mechanism for the pristine membrane ( $R^2 = 0.374$ ). Coating the ceramic membrane increased its hydrophilicity, as established through contact angle measurements, which showed a 23% decline in hydrophobicity from uncoated to coated membrane.

## ACKNOWLEDGEMENTS

The authors are grateful for funding received from the National Research Foundation, South Africa (NRF), and the University of South Africa.

## SUPPLEMENTARY MATERIAL

The Supplementary Material for this paper is available online at <https://dx.doi.org/10.2166/wst.2019.419>.

## REFERENCES

- Angelis, L. D., Marta, M. & Cortalezzi, F. D. 2013 Ceramic membrane filtration of organic compounds: effect of concentration, pH, and mixtures interactions on fouling. *Separation and Purification Technology* **118**, 762–775. doi: 10.1016/j.seppur.2013.08.016.
- Chaukura, N., Moyo, W., Mamba, B. B. & Nkambule, T. I. 2018 Removal of dissolved organic matter from raw water using zero valent iron-carbonaceous conjugated microporous polymer nanocomposites. *Physics and Chemistry of the Earth* **107**, 38–44. doi: 10.1016/j.pce.2018.08.006.
- Kim, H. C. & Dempsey, B. A. 2013 Membrane fouling due to alginate, SMP, EfOM, humic acid, and NOM. *Journal of Membrane Science* **428**, 190–197. doi: 10.1016/j.memsci.2012.11.004.
- Kim, K. & Jang, A. 2016 Fouling characteristics of NOM during the ceramic membrane microfiltration process for water treatment. *Desalination and Water Treatment* **3994**, 1–9. doi: 10.1080/19443994.2015.1057035.
- Mahlangu, T. O., Msagati, T. A. M., Hoek, E. M. V., Verliefe, A. R. D. & Mamba, B. B. 2015a Rejection of pharmaceuticals by nanofiltration (NF) membranes: effect of fouling on rejection behaviour. *Physics and Chemistry of the Earth, Parts A/B/C* **76**, 28–34. doi: 10.1016/j.pce.2014.11.008.
- Mahlangu, T. O., Thwala, J. M., Mamba, B. B., D'Haese, A. & Verliefe, A. R. D. 2015b Factors governing combined fouling by organic and colloidal foulants in cross-flow nanofiltration. *Journal of Membrane Science* **491**, 53–62. doi: 10.1016/j.memsci.2015.03.021.
- Metsämuuronen, S., Silanpao, M., Bhatnagar, A. & Manttari, M. 2014 Natural organic matter removal from drinking water by membrane technology. *Separation and Purification Technology* **43**, 1–61. doi: 10.1080/15422119.2012.712080.
- Motsa, M. M., Mamba, B. B., D'Haese, A., Hoek, E. M. V. & Verliefe, A. R. D. 2014 Organic fouling in forward osmosis membranes: The role of feed solution chemistry and membrane structural properties. *Journal of Membrane Science* **460**, 99–109. doi: 10.1016/j.memsci.2014.02.035.
- Motsa, M. M., Mamba, B. B. & Verliefe, A. R. D. 2015 Combined colloidal and organic fouling of FO membranes: the influence of foulant-foulant interactions and ionic strength. *Journal of Membrane Science* **493**, 539–548. doi: 10.1016/j.memsci.2015.06.035.
- Motsa, M. M., Mamba, B. B. & Verliefe, A. R. D. 2018 Forward osmosis membrane performance during simulated wastewater reclamation: fouling mechanisms and fouling layer properties. *Journal of Water Process Engineering* **23**, 109–118. Elsevier. doi: 10.1016/j.jwpe.2018.03.007.

- Ndiweni, S. N., Chys, M., Chaukura, N., van Hulle, S. W. H. & Nkambule, T. T. I. 2019 Assessing the impact of environmental activities on natural organic matter in South Africa and Belgium. *Environmental Technology* **40** (13), 1756–1768. doi: 10.1080/09593330.2019.1575920.
- Nguyen, T., Roddick, F. A. & Fan, L. 2012 Biofouling of water treatment membranes: a review of the underlying causes, monitoring techniques and control measures. *Membranes* **2** (4), 804–840. doi: 10.3390/membranes2040804.
- Nkambule, T. I. 2012 *Natural Organic Matter (Nom) in South African Waters: Characterization of Nom, Treatability and Method Development for Effective Nom Removal From Water*. PhD Thesis, University of Johannesburg.
- Puhlfürß, P., Voigt, A., Weber, R. & Morbe, M. 2000 Microporous TiO<sub>2</sub> membranes with a cut off <500da. *Journal of Membrane Science* **174**, 123–133.
- Rubia, A., Rodriguez, M., Leon, V. & Prats, D. 2008 Removal of natural organic matter and THM formation potential by ultra- and nanofiltration of surface water. *Water Research* **42**, 714–722. doi: 10.1016/j.watres.2007.07.049.
- Schulz, M., Soltani, A., Zheng, X. & Ernst, M. 2016 Effect of inorganic colloidal water constituents on combined low-pressure membrane fouling with natural organic matter (NOM). *Journal of Membrane Science* **507**. doi: 10.1016/j.memsci.2016.02.008.
- Shang, R., Vuong, F., Hu, J., Li, S., Kemperman, A. J. B., Nijmeijer, K., Corneissen, E. R., Heijman, S. G. J. & Rietveld, L. C. 2015 Hydraulically irreversible fouling on ceramic MF/UF membranes: comparison of fouling indices, foulant composition and irreversible pore narrowing. *Separation and Purification Technology* **147**, 303–310. doi: 10.1016/j.seppur.2015.04.039.
- Shang, R., Goulas, A., Tang, C., Frias Serra, X., Rietveld, L. C. & Heijman, S. G. J. 2017 Atmospheric pressure atomic layer deposition for tight ceramic nanofiltration membranes: synthesis and application in water purification. *Journal of Membrane Science* **528**, 163–170. doi: 10.1016/j.memsci.2017.01.023.
- Shao, S., Liang, H., Qu, F., Yu, H., Li, K. & Li, G. 2014 Fluorescent natural organic matter fractions responsible for ultrafiltration membrane fouling: identification by adsorption pretreatment coupled with parallel factor analysis of excitation-emission matrices. *Journal of Membrane Science* **464**, 33–42. doi: 10.1016/j.memsci.2014.03.071.
- Shen, J. & Schaffer, A. I. 2015 Factors affecting fluoride and natural organic matter (NOM) removal from natural waters in Tanzania by nanofiltration/reverse osmosis. *Science of the Total Environment* **527–528**, 520–529. doi:10.1016/j.scitotenv.2015.04.037.
- Song, Z., Fathizadeh, M., Huang, Y., Chu, H. K., Yoon, Y., Wang, L., Xu, L. W. & Yu, M. 2016 TiO<sub>2</sub> nano filtration membranes prepared by molecular layer deposition for water purification. *Journal of Membrane Science* **510**, 72–78. doi:10.1016/j.memsci.2016.03.011.
- Sun, W., Nan, J., Xing, J. & Jian, J. 2016 Identifying the major fluorescent components responsible for ultrafiltration membrane fouling in different water sources. *Journal of Environmental Science* **45**, 215–223. doi:10.1016/j.jes.2016.01.007.
- Wang, H., Ding, A., Gan, Z., Qu, F., Cheng, X., Bai, L., Guo, S., Li, F. & Liang, H. 2017 Fluorescent natural organic matter responsible for ultra filtration membrane fouling: fate, contributions and fouling mechanisms. *Chemosphere* **182**, 183–193. doi: 10.1016/j.chemosphere.2017.04.148.
- Yamamura, H., Okimoto, Y., Kimura, K. & Watanabe, Y. 2014 Hydrophilic fraction of natural organic matter causing irreversible fouling of microfiltration and ultrafiltration membranes. *Water Research* **54**, 123–136. doi: 10.1016/j.watres.2014.01.024.
- Yu, H., Chang, H. & Shao, X. 2015 Understanding ultrafiltration membrane fouling by soluble microbial product and effluent organic matter using fluorescence excitation-emission matrix coupled with parallel factor analysis. *International Biodeterioration and Biodegradation* **102**. doi: 10.1016/j.ibiod.2015.01.011.
- Zularisam, A. W., Ismail, A. F., Salim, M. R., Sakinah, M. & Ozaki, H. 2007 The effects of natural organic matter (NOM) fractions on fouling characteristics and flux recovery of ultrafiltration membranes. *Desalination* **212** (1–3), 191–208. doi: 10.1016/j.desal.2006.10.010.

First received 4 July 2019; accepted in revised form 7 December 2019. Available online 23 December 2019